



Long-Term Modeling of Soil Moisture Dynamic in Response to Land-Use/Cover Changes: A Case Study in the Telo Watershed of Tehran, Iran

ARTICLE INFO

Article Type Original Research

Authors

Jahangir Porhemmat, Ph.D.^{1*}
Seyed Mohammad Tajbakhsh, Ph.D.²
Majid Altafi Dadgar, Ph.D.³
Abdolnabi Abdeh Kolahchi, Ph.D.⁴

How to cite this article

Porhemmat J., Tajbakhsh SM., Altafi Dadgar M., Abdeh Kolahchi A. Long-Term Modeling of Soil Moisture Dynamic in Response to Land-Use/Cover Changes: A Case Study in the Telo Watershed of Tehran, Iran. ECOPERSIA 2025;13(2): 199-219.



10.22034/ECOPERSIA.13.2.199

¹ Professor, Soil Conservation and Watershed Management Research Institute (SCWMRI), Agricultural Research, Education and Extension Organization (AREEO), Tehran, Iran

² Associate Professor, Birjand University, Birjand Iran.

³ Ph.D. Groundwater and Geothermal Research Center (GRC), Water and Environment Research Institute, Ferdowsi University of Mashhad, Iran.

⁴ Assistant Professor, Soil Conservation and Watershed Management Research Institute (SCWMRI), Agricultural Research, Education and Extension Organization (AREEO), Tehran, Iran.

* Correspondence

Address: Professor, Soil Conservation and Watershed Management Research Institute (SCWMRI), Agricultural Research, Education and Extension Organization (AREEO), Tehran, Iran.
Tel: +989123902521
Email: porhemmat@scwmri.ac.ir

Article History

Received: March 7, 2025

Accepted: May 10, 2025

Published: March 13, 2025

ABSTRACT

Aims: Soil moisture (SM) dynamic is crucial in water resources management. This is complicated by the variability of Land-use (LU) and land cover (LC) at the watershed scale, which is the focus of this research.

Materials & Methods: SM was measured at five depths across seven stations within three LU/LC types to calibrate the HYDRUS-1D model. The calibrated model was then used to simulate SM dynamic and investigate the soil water balance components in the different LU/LC types from early 2007 to late 2021. To verify the model, R² is above 0.80, with a significance level of 5%.

Findings: The amount of drainage from the lower root zone was 10, 4, and 7.3 cm for rangeland, tree, and bare soils, respectively. The results show infiltration was 42, 62, and 41 cm, and evapotranspiration was 317, 574, and 345 mm. This indicates that the highest infiltration and SM storage occurred in tree land, drainage from the root zone in rangeland, and surface evaporation from the bare soils.

Conclusion: The result indicates that tree-dominated LU/LC increases infiltration and soil moisture storage capacity compared to other LU/LC types. Evaporation and direct runoff losses from bare soils are greater than those from rangeland and tree-dominated LU/LC. Furthermore, deep percolation is higher in rangeland than in tree-covered areas and bare land. In conclusion, LU/LC significantly influences water balance components and soil water dynamic, highlighting the importance of considering LU/LC in water resource and consumption management.

Keywords: Evapotranspiration; HYDRUS-1D; Infiltration; Land-use Management; Soil Moisture Modeling; Unsaturated Zone.

CITATION LINKS

[1] Hu W., Shao M.A., Hou M.T., ... [2] Vereecken H., Huisman J.A., ... [3] Rasheed M.W., Tang J., Sarwa ... [4] Ye N., Walker J.P., Gao Y., ... [5] Zhang M., Zhang D., Jin Y., ... [6] Widyastuti M.T., Padarian J. ... [7] Bakhshian S., Zarepakzad N., ... [8] Ursulino B.S., Montenegro S. ... [9] Duarte E., Hernandez A. A re ... [10] Vereecken H., Huisman J.A., ... [11] Bai X., Jia X., Jia Y., Shao ... [12] Cantón Y., Solé-Benet A., D ... [13] Jafarian Jeloudar Z., Shaban ... [14] Shen M., Zhang J., Zhang S., ... [15] Jia X., Wang Y., Shao M., Lu ... [16] Afshari M., Hashemi S.S., At ... [17] Jia X., Zhao C., Wang Y., Zh ... [18] Porhemmat J., Nakhaei M., Al ... [19] Altafi Dadgar M., Nakhaei M. ... [20] Garcia-Prats A., del Campo A ... [21] Jarvis N. J. Simulation of s ... [22] Jarvis N.J., Messing I. Near ... [23] Jarvis N.J., Hollis J.M., Ni ... [24] Fechter J., Allison B.E., Si ... [25] J.G., Feddes R.A., Kabat P., ... [26] Van Dam J.C. Field scale wat ... [27] Hutson J.L., Wagenet R.J. LE ... [28] Hutson J. L., Wagenet R.J. S ... [29] Hutson J.L. Leaching Estim ... [30] Asada K., Eguchi S., Urakawa ... [31] Šimůnek J., Šejna M., van Ge ... [32] Šimůnek J., van Genuchten M. ... [33] Šimůnek J., Šejna M., van Ge ... [34] Šimůnek J., Šejna M., Saito ... [35] Šimůnek J., Van Genuchten M. ... [36] Šimůnek J., Šejna M., Saito ... [37] Šimůnek J., van Genuchten M. ... [38] Radcliffe D.E., Šimůnek J. S ... [39] Richards Lisa A. Capillary c ... [40] Abbasi F., Adamsen F.J., Hun ... [41] Wang F.X., Kang Y., Liu S.P. ... [42] Skaggs T.H., Trout T. J., Š ... [43] Wöhling T. Seasonal Furrow I ... [44] Siyal A.A., Skaggs T.H. Meas ... [45] Patel N., Rajput T.B.S. Dyna ... [46] Cheng X., Huang M., Si B.C., ... [47] Essig E.T., Corradini C., Mo ... [48] Guan H., Šimůnek J., Newman ... [49] Wang H., Tetzlaff D., Soulsb ... [50] Besharat S., Nazemi A.H., ... [51] Altafi Dadgar M., Nakhaei M. ... [52] Noorabadi S., Sadraddini S.A ... [53] Xiaoxu J., Shao M., Zhu Y., ... [54] Elnesr M.N., Alazba A.A. Com ... [55] Forkutsa I., Kaas R.S. Shiro ... [56] Šimůnek J., van Genuchten M. ... [57] Xie T., Liu X., Sun T. The e ... [58] Djabelkhir K., Lauvernet C., ... [59] Hu W., Wang Y.Q., Li H.J., H ... [60] Guo Y., Fang G., Xu Y P., Ti ... [61] Zhang C., Wang Y., Jia X., S ... [62] Porhemmat J., Altafi-Dadgar ... [63] Grossman R.B., Reinsch T.G. ... [64] Dane J.H., Hopmans J.W. Pres ... [65] Gee G.W., Or D. Particle siz ... [66] Feddes R.A., Kowalik P.J., Z ... [67] Van Genuchten M.Th. A closed ... [68] Mualem Y. A new model for pr ... [69] Turkeltaub T., Kurtzman D., ... [70] Kashyap P.S., Panda R.K. Eva ... [71] Allen R.G., Pereira L.S., Ra ... [72] Jiménez-Martínez J., Skaggs ... [73] Schaap M.G., Leij F.J., van ... [74] Zhao M., Wang W., Ma Z., Wan ...

Introduction

Soil moisture (SM), as the main factor of energy and water flux in the soil layers, is an essential variable in hydrological and land surface processes [1,2,3,4,5,6], is a crucial factor in land-atmosphere interactions [7] and directly influencing hydrological water balance components [8,9]. SM has also been mentioned as a fundamental parameter in the stability and health of global ecosystems in regions with limited water resources and seasonal water shortages [10,11]. In addition, it is spatially and temporally heterogeneous, which is controlled by different factors such as soil surface cover [12], vegetation type [13,14], and so on. The SWC dynamic depend closely on climate and Land-use (LU) types. Climatic changes and LU variation can change the conditions of SM content in the surface and deeper soil layers [15], affecting plant growth, material transport, and biogeochemical cycles in the earth's ecosystems [16,17]. Therefore, recognizing long-term changes in SWC under the influence of LU changes will be necessary and proper for water management, particularly in areas with limited water resources [17]. On the other hand, due to population growth and increased demand for food supply, agricultural development is almost impossible despite the lack of water resources. Therefore, preventing water wastage in the irrigation process is one of the most critical priorities of agricultural management. Studying changes in the SM profile allows for identifying the best irrigation management method [18]. The variability of conductivity and physical characteristics of soil layers is challenging in studying water movement in the soil profile [19]. The water movement in the soil profile as a porous medium has been studied for many years in different countries. Despite this, SM routing faces many unknowns for optimal irrigation management because of SM's high spatial and temporal distribution changes in

the unsaturated zone. In addition, knowing the variation of SM in the subsurface and lower depth of the soil profile is a time-consuming and expensive field operation, which has many limitations in terms of financial, physical, and practical conditions, which will be more complicated over the watershed natural conditions. The direct measurements of SM are expensive and only represent a limited area; thus, they mainly depend on the spatial variation of physical soil properties [20]. Therefore, integrated studies, including field studies and experimental data with numerical modeling, are reliable for such investigations. Knowledge of the water movement process in the soil profile is not only an essential factor for choosing the type and method of irrigation but also an essential factor in determining the water balance components and water resources management. Soil profile is a critical and fundamental boundary layer between surface and groundwater resources. The SM content data in the soil profile provides the necessary information for optimal management of water consumption, especially in agriculture [19].

There are several models for simulating the water movement and solutes, such as MACRO models [21, 22, 23], SWAP [24, 25, 26], LEACHM [27-30], and HYDRUS [31-38]. The HYDRUS is one of the advanced models with the ability to simulate three-dimensional water, solute, and heat movements in saturated and unsaturated conditions by solving Richard's equation [39]. It can also simulate water absorption by the roots and root growth in the above conditions. This model was developed by Šimůnek et al. (1999) [31] at the American Soil Salinity Laboratory [31]. In addition, the HYDRUS model can also estimate the physical properties of the soils by using the optimization method with reverse implementation [33]. The HYDRUS model has been used to simulate or inversely estimate

soil hydraulic parameters in many laboratory and field studies ^[40, 41]. Skaggs et al. (2004) ^[42] demonstrated that simulations using the HYDRUS model closely matched the details of field measurements and observations for drip irrigation. Wöhling (2005) ^[43] simulated the infiltration rate from the furrow by selecting a section to estimate the contour lines of the moisture contents and moisture distribution in that section. Siyal and Skaggs (2009) ^[44] Evaluation of the capability of the HYDRUS in predicting the SM distribution pattern in subsurface drip irrigation. The model could simulate the moisture front in a subsurface drip irrigation well (the coefficient of determination was more than 0.97). Patel and Rajput (2008) ^[45] studied a drip irrigation system in an onion farm; the main goal was to apply the HYDRUS model in simulating SM. The model's simulated SM distribution results were correlated more closely with the measured data, with no statistically significant difference. Based on this research, Patel and Rajput (2008) ^[45] recommended using this model to design subsurface drip irrigation systems to minimize the deep infiltration rate from the bottom of the soil layers. Several researchers have used the HYDRUS model to simulate saturated conditions ^[46]. For example, Essig et al. (2009) ^[47] modeled the infiltration rate and the amount of deep percolation in a saturated sloping soil and compared it with the laboratory results. The results of this research show the capability of the HYDRUS model in estimating deep percolation of saturated environments. Guan et al. (2010) ^[48] used the HYDRUS model to evaluate the effects of vegetation root distribution on near-surface water partitioning. Wang et al. (2018) ^[49] used the HYDRUS-1D model to quantify the soil water balance in land-cover and potential climate change impacts. They concluded that evapotranspiration would increase and deep percolation to

recharge groundwater would decrease by land-cover changes from Shrubs to trees, respectively. Besharat et al. (2011) ^[50] showed that the maximum water absorption rate is at a depth of 25 to 30 cm and the minimum absorption is at a depth of 80 cm by comparing the SM obtained from the simulation of the HYDRUS model and the SM data obtained from the field measurements. Altafi Dadgar et al. (2018) ^[51] used the HYDRUS-1D software package to evaluate soil water dynamic and return water from different irrigation systems. The differences in soil water balance components between homogeneous and nonhomogeneous soils in pastures were investigated by Cheng et al. (2013) ^[46]. The results indicate that annual water balance components are significantly affected by soil layering. They found that actual transpiration in layered soils was greater than in homogeneous soils. A comparison of the SIRMOD and HYDRUS has been done by Noorabadi et al. (2014) ^[52]. The results indicated that the comprehensive hydrodynamic model in SIRMOD demonstrated a strong capability to predict all phases of irrigation, particularly the advanced phase. In contrast, the HYDRUS-3D model simulated the infiltrated water volume and outflow hydrograph more accurately than the SIRMOD model. Xiaoxu et al. (2017) ^[53] used the HYDRUS model to investigate the effects of forest planting in areas of China on soil water dynamic. Their research showed that planting the non-native tree species had adverse effects on SM content because decreasing moisture in the soil will lead to dryness in the surface and even deep layers. Also, comparing the water moisture content in the soil in the areas where forestry has become non-native, it was much less than the areas covered by pasture species. The HYDRUS model has been utilized to assess the efficiency and uniform distribution of irrigation systems in various

studies, including Elnesr and Alazba (2019)^[54], who employed this model to evaluate the accuracy and stability of the surface drip irrigation system. Several studies have used this model to analyze salinity, nutrient transport, SM, and plant growth issues^[55-58]. Porhemmat et al. (2018)^[18] investigated the effects of different irrigation systems on the amount of drainage from the root zone of the plant by using the HYDRUS model. This research showed that the model could simulate water movement and soil suction and estimate drainage rates from different irrigation systems. The HYDRUS model was used to investigate the effects of soil, vegetation, and climate on potential groundwater recharge (GR) at a regional scale Hu et al. (2019)^[59]. Altafi Dadgar et al. (2020)^[19] simulated the groundwater recharge potential in the unsaturated zone with the HYDRUS model. In this study, the model was calibrated along the 10-meter soil profile with a determination coefficient of 94%. This research showed that most rainfall does not drain deeply, and only the combined effect of rainfall and irrigation, or successive rainfalls, has a significant deep drain. Guo et al. (2020)^[60] simulated the effects of LU changes on SM content in a region of China. This research showed that dry soil can retain moisture up to 4 meters deep over time by changing vegetation. Also, some pasture species can make the soil profile drier than the other species. Zhang et al. (2020)^[61] investigated the effects of rainfall and land regeneration on the plant's available water storage in the root zone. This research showed that changing the type of plant species to native species increases the available water storage for plants. Another result is that planting tree species instead of pasturing reduces saturated moisture in the root zone. Research findings indicate that the HYDRUS model provides sufficient accuracy for simulating water movement in saturated

and unsaturated soil profiles and soil water balance components at the basin scale. Existing research demonstrates that most SM studies have been limited to the farm scale. Furthermore, the impact of varying natural LC and LU on SM dynamic remains unclear. Consequently, this research utilizes the HYDRUS model to evaluate long-term soil water balance concerning changes in LC/LU across the watershed scale. Therefore, the Telo region was selected for this research because of its characteristics and conditions, such as its basin scale, vegetation diversity, and soil moisture.

Materials & Methods

Study Area

The study area is located northeast of Tehran city in Iran, with an area of 3.28 km². Telo is located between 35° 47' 6" to 35° 48' 15" N and 51° 37' 8.3" to 51° 39' 17" E (Figure 1). The altitude of this area ranges from 1613 m to 1971 m above sea level. The climate condition is semi-arid, with a mean rainfall of 457 mm, of which 41%, 27%, 26%, and 6% are in winter, autumn, spring, and summer, respectively. The study area is widely covered by rangeland plants, which have a high density, and pine and cypress tree species and some other forest species are also observed. The mean annual temperature ranges between 12.1 °C to 13.2 °C from upper to lower parts, and the annual mean of the potential evapotranspiration is 1337 mm over the watershed. The mean temperature variation is below zero in January up to 25 °C in late July over the watershed. There are three geological formations, from cretaceous to recent, named Lar, Fajan, and Karaj, with volcanic rocks and young alluvial sediments. Lar formation consists of thin-layered micrite limestones with a gray color covering a small part of the northern side. The Fajan conglomerate formation is exposed in a

small part of the north and northeast of the study area with a discontinuity on the Lar formation. Karaj formations that consist of a sequence of green tuffs, sedimentary rocks, volcanic lavas, and rarely evaporites occupy a considerable part of the study area. The fourth outcrop is volcanic rocks, mainly located in several horizons of the Karaj formation or directly exposed in the eastern area. Finally, young alluvial sediments with moderate sorting originated from Karaj Formation erosion at the bottom of the valleys. The soil surveying results indicate that most soils have evolved soil horizons with medium to heavy textures in this basin. The soil characteristics do not have a complete horizon, and there is some chalk in the soil texture in the southern part, where there are evaporite formations, sandstone, and marl. The results of the vegetation cover study in the Telo area (SCWMRI, 2018) show

that 81%, 12.2%, and 6.8% of the total area are covered by vegetation, bare soil, rocks, and gravel, respectively. Therefore, LC and LU can be divided into three categories, including rangeland, tree cover, and bare soil.

Data Collection

The soil moisture dynamic modeling requires various climate data, including precipitation, evaporation, temperature, humidity, and wind. Lavasan and Latyan Dam meteorological stations, 3 and 4.2 Km away from the watershed center and located in the north and the east of this area (belong to the Meteorology Organization of IR Iran), respectively, are used as historical data. Modeling of the soil moisture dynamic requires calibration using observation data. For this purpose, 6 points of the area with the same soil depth but different LU and LC (Table 1) were selected to collect data

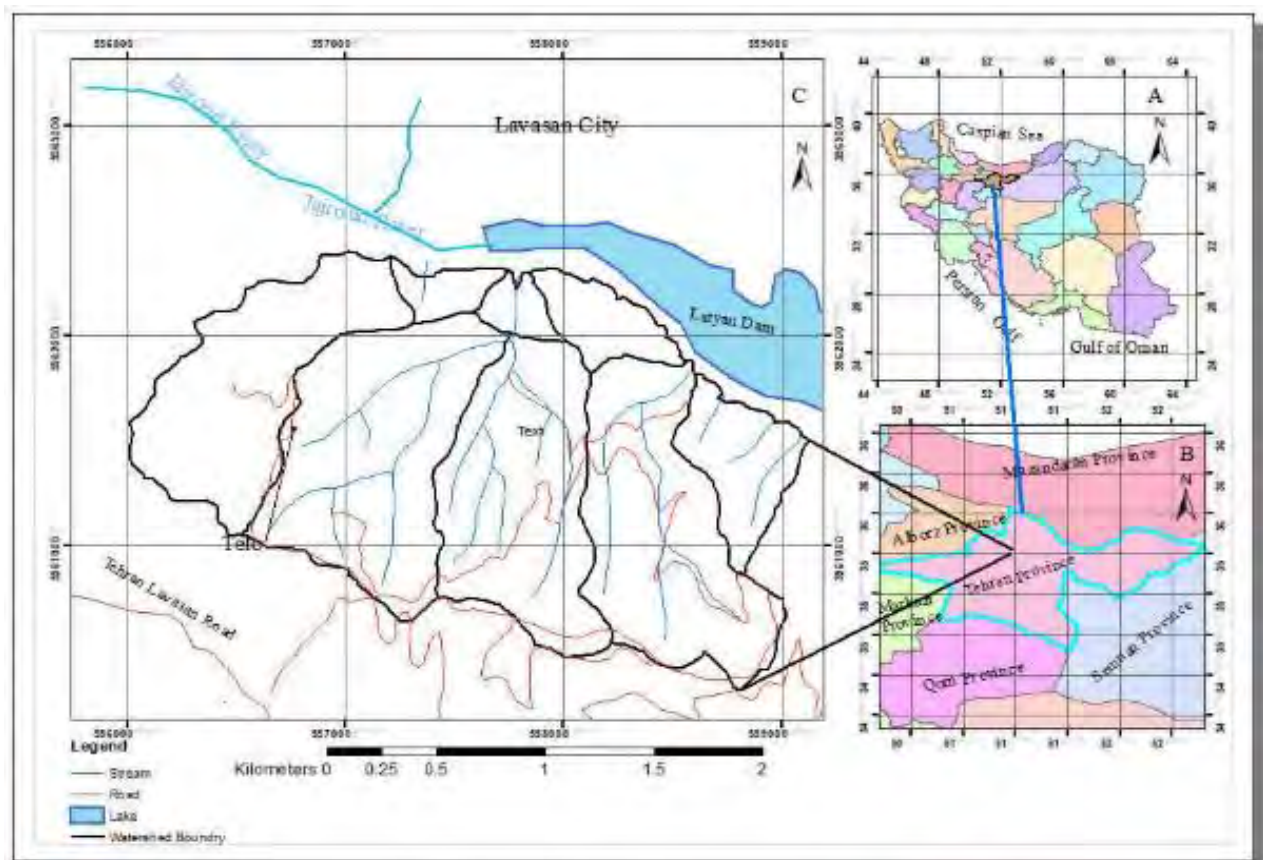


Figure 1) Location of study area (A: Iran, B: Tehran Province, and C: Study area).

Table 1) LC/LU of different stations over the study area.

Station	P1	P2	P3	P4	P6	P7
LC/LU	Rangeland	Rangeland	Rangeland	Pine Trees	Rangeland	Bare Soil

Table 2) Soil texture profiles in the root zone of the study area exhibit varying textures across the watershed.

No	Sample	Sand (%)	Silt (%)	Clay (%)	Texture
1	P3-1	65.43	21.56	13.01	Sandy Loam
2	P3-2	38.52	31.38	30.10	Clay Loam
3	P4-1	15.02	39.09	45.89	Clay
4	P4-2	7.16	40.56	52.29	Silty Clay
5	P6-1	16.65	47.19	36.16	Silty Clay Loam
6	P6-2	15.05	44.37	40.58	Silty Clay
7	P7-1	24.75	45.55	29.70	Clay Loam
8	P7-2	30.17	38.99	30.84	Clay Loam

[62]. These points were selected based on the amount of moisture in the rangeland area and near the root zoon of tree species. A profile probe device (PR2) was used to Measure SM at a depth of 10, 20, 30, 40, 60, and 100 cm from the surface simultaneously at seven stations in different watershed parts (P1 to P7). The SM content was collected at seven monitoring sites for 1.5 years, from October 2018 to April 2022. Physical soil factors were determined using samples collected from the soil profile excavated near the PR2 location, taken from 1 meter top of the soil. Then, soil bulk density [63], soil water retention curve [64], soil texture [65], and soil particle size distribution curve were determined in a laboratory using the results of soil sample analysis. Table 2 shows the results of soil texture in the root zone of the selected sites based on the soil sample analysis.

Numerical Model Simulations

The HYDRUS-1D model was employed to simulate flow within the soil profile and the water absorption by plant roots in soil with varying SM contents by numerically

solving Richard's equation. Consequently, the assumptions are: each soil layer is homogeneous and isotropic, the air phase does not influence the flow process, and the effects of gradient and temperature variation are negligible. In this context, the governing equation for the water movement will take the form of a one-dimensional Richards equation (Eq. 1), which is solved using the Galerkin finite element method:

$$\frac{\partial \theta}{\partial t} = \frac{\partial}{\partial z} \left[k \left(\frac{\partial h}{\partial z} + 1 \right) \right] - s(z, t) \quad \text{Eq. (1)}$$

In Eq. (1), h is suction head (L), θ is water content in ($L^3.L^{-3}$), t is time (T), K is hydraulic conductivity ($L.T^{-1}$), z is vertical coordination (L), and $S(z,t)$ is sink term (ST) known as plant root absorb water ($L^3.L^{-3}.T^{-1}$).

The ST could be determined by the potential rate of water absorption of the plant and a stress factor [66]:

$$s(h) = \alpha(h) \cdot S_p \quad \text{Eq. (2)}$$

In Eq. (2), S_p is the ST in Eq. (1), $\alpha(h)$ is a dimensionless function of response to

stress that describes the reduction of water absorption by roots in dry conditions, and its value is variable between zero and one ($0 \leq \alpha \leq 1$) introduced by Feddes et al. (1978) [66] as below:

$$\alpha(h) = \begin{cases} \frac{h-h_4}{h_3-h_4}, h_4 < h \leq h_3 \\ 1, h_4 < h \leq h_3 \\ \frac{h-h_1}{h_2-h_1}, h_2 < h \leq h_1 \\ 0, h \leq h_4 \text{ or } h > h_1 \end{cases} \quad \text{Eq. (3)}$$

h_1 , h_2 , h_3 and h_4 are limit parameters. When the pressure load around the plants' root is between h_2 and h_3 , the absorbed water by the roots will be at the high-level rate (S_p), and when the head is more than h_2 or less than h_3 , it will linearly decrease. If the pressure load is less than h_4 and more than h_1 , the absorbed water by the roots tends to zero. The limit values for each plant can be used and extracted from the reference data available in HYDRUS-1D. In the current study, the values of h_1 , h_2 , h_3 , and h_4 are as follows: $h_1 = -10$ cm, $h_2 = -25$ cm, $h_3 = -800$ cm, $h_4 = -8,000$ cm, according to the type of vegetation of the area, which consists of rangeland plants and pine tree species. Parameters of the soil hydraulic were modeled by Eq. (4), which is a combined function of Van Genuchten-Mualem [67, 68] as follows:

$$\alpha(h) = \begin{cases} \left\{ \theta_r + \frac{\theta_s - \theta_r}{(1 + |\alpha \cdot h|^n)^{\frac{1}{1+\frac{1}{n}}}} \right\} \text{ for } h < 0 \\ \theta_s \text{ for } h \geq 0 \end{cases} \quad \text{Eq. (4)}$$

$$k(h) = k_s \cdot S_e^l \left[1 - \left(1 - S_e^{\frac{n}{n-1}} \right)^{1 - \frac{1}{n}} \right]^2 \quad \text{Eq. (5)}$$

$$S_e = \frac{\theta(h) - \theta_r}{\theta_s - \theta_r} \quad \text{Eq. (6)}$$

where θ_s represents the volumetric water

content (VWC) of saturated soil ($L^3.L^{-3}$), θ_r denotes the residual soil VWC ($L^3.L^{-3}$), K_s indicates the unsaturated hydraulic conductivity ($L.T^{-1}$), S_e is the effective saturation, and α , n , and l are empirical parameters that define the form of hydraulic functions. To decrease the parameters of these equations, the value of l is considered as 0.5 based on the common assumption of Mualem (1976) [68] and Turkeltaub et al. (2015) [69]. HYDRUS-1D software uses the Galerkin finite element method to solve Eq. (3) to Eq. (5). The atmospheric boundary conditions were considered at the surface. In contrast, free drainage conditions were considered between the drainage and soil layers at the bottom of the model. These conditions were applied, assuming the drainage layer was not saturated with water [32].

Evapotranspiration (ET)

Implementing atmospheric boundary conditions in the model requires determining the amount of irrigation and daily rainfall and the potential evapotranspiration or ETp (t) ($L.T^{-1}$) rate. To determine evaporation and transpiration, the reference ET ($ET_0(t)$) was first calculated using the Penman-Mantis equation [70]. Then, the ETp was calculated using Eq. 7 [71].

$$ET_p(t) = K_c(t) \cdot ET_0(t) \quad \text{Eq. (7)}$$

$ET_0(t)$ is discretized daily, and $K_c(t)$ denotes a crop coefficient that reflects the water absorption and evaporation by the crop about the crop reference. Allen et al. (1998) [71] provided data on the duration of growth stages and K_c values for various crops. The crop coefficients of rangeland plants were extracted from existing tables [71] for the growth stages (Table 3). After calculating ETp from Eq. (7), the potential evaporation can be calculated based on Eq. (8).

$$E_p = ET_p \cdot \exp^{-\beta \cdot LAI} \quad \text{Eq. (8)}$$

Table 3) Growth stage duration and crop coefficient at each stage^[71] used for estimating actual evapotranspiration.

Crop Type	Growing Stage (days)				Crop Coefficient (Kc)		
	Initial	Development	Mid	Late	Initial	Mid	Ending
Rangeland	10	30	25	10	0.4	0.95	0.8

where $\beta \approx 0.4$ is the radiation attenuation coefficient, and LAI is the leaf area index. Due to the lack of information regarding (LAI) to separate potential evaporation from potential evapotranspiration, the following relationship was used ^[72]:

$$E_p = ET_p \cdot f(t) \quad \text{Eq. (9)}$$

where $f(t)$ is determined from some assumptions. These assumptions mean there is no vegetation, potential evaporation at its maximum value, and transpiration is zero ($f(t)=1$) When the crop has been planted. On the contrary, when the crop reaches the middle stage of its growth, the vegetation is complete, the evaporation is almost zero, and $f(t)=0$. All other stages, from the growth time to the crop harvest, will vary between the values of $f(t)=1$ at the planting stage and $f(t)=0$ at the beginning of the middle stage of growth. Since plant growth follows an S-shaped pattern, the transition zone between the two limit values can be extracted using a sigmoid curve (S-shaped). In this way, the potential evaporation and the potential transpiration are extracted by subtracting the potential evaporation from the potential evapotranspiration. Then the data from the Lavasan synoptic and Latyan climatic stations were used to calculate evapotranspiration.

Model Preparation and Calibration

Several layers of information are required to run the HYDRUS model. The most important layers are the boundary conditions, such as rainfall, irrigation, and potential evapotranspiration rates. Also, the other required data are

physical and hydraulic parameters of the soil in the Van Genuchten-Mualem model, as well as the observational data of the SM. The boundary conditions have been chosen as the atmospheric conditions at the model surface by using observed data, including rainfall, daily transpiration, and irrigation at these surfaces. Figure 2 shows the values of rainfall (P), daily evaporation (E_p), and transpiration (T_p) for 15 years from 2007 to 2021. The separation of transpiration from evapotranspiration values has been done using the S model in the materials and methods chapter. The selected sites were irrigated four times in the dry season from October 2020 to the end of 2021 in the pan around the tree species. The model was calibrated in 15 months, from October 2020 to the end of 2021, and the SM was measured during this period. Then, the SM dynamic were simulated for 15 years, from 2007 to 2021, based on the observed meteorological data. As mentioned in the previous chapters, SM dynamic modeling requires the parameters of Van Genuchten-Mualem equations, which are extracted using Rosetta software as initial values for modeling ^[73,35]. Table 4 shows the parameters related to the soil water retention curve. Figures 3 to 6 show the correlation of simulated and observed SM in the calibration stage for a few samples in the selected stations. In addition, Table 5 shows the correlation coefficient between simulated and observed SM at different sites due to the calibration of the model.

Findings

The present research investigated the SM dynamic on the watershed scale. The

Table 4) Input values of soil-water retention curve parameters in the Hydrus model.

Station Code	θ_r (cm ³ .cm ⁻³)	θ_s (cm ³ .cm ⁻³)	α (cm ⁻¹)	n (-)	Ks (cm.d ⁻¹)
P3-1	0.047	0.385	0.030	1.392	33.760
P3-2	0.070	0.384	0.015	1.349	4.280
P4-1	0.097	0.485	0.014	1.340	15.510
P4-2	0.091	0.418	0.014	1.280	2.700
P6-1	0.091	0.471	0.010	1.450	12.600
P6-2	0.089	0.431	0.011	1.391	4.840
P7-1	0.081	0.445	0.008	1.496	12.320
P7-2	0.064	0.341	0.015	1.281	1.700

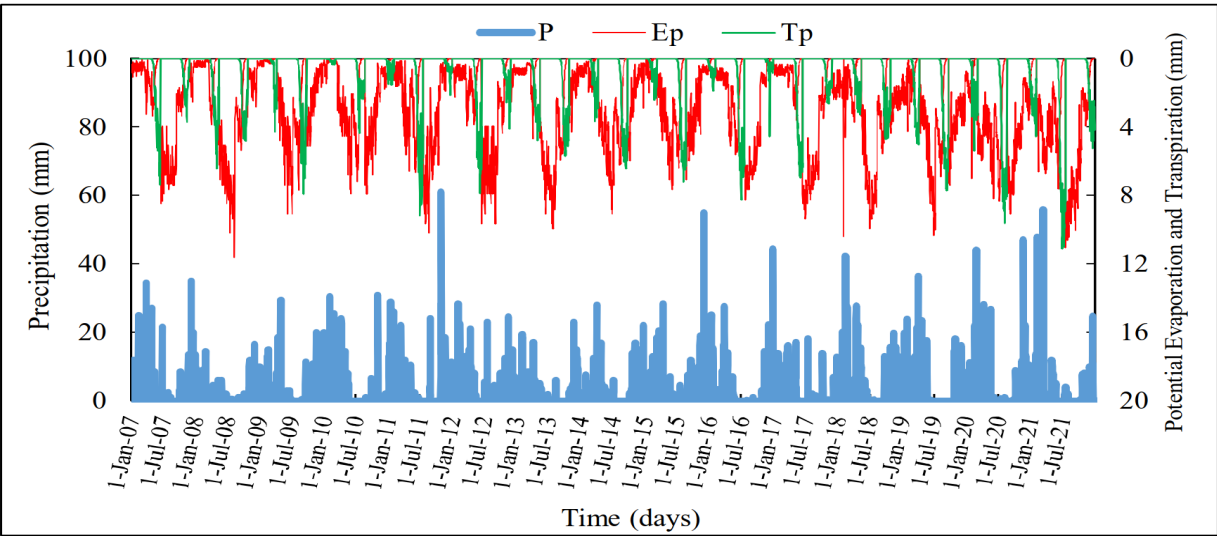


Figure 2) Daily rainfall (P), evaporation (E_p), and transpiration (T_p) values from 2007 to 2021 as boundary conditions for modeling.

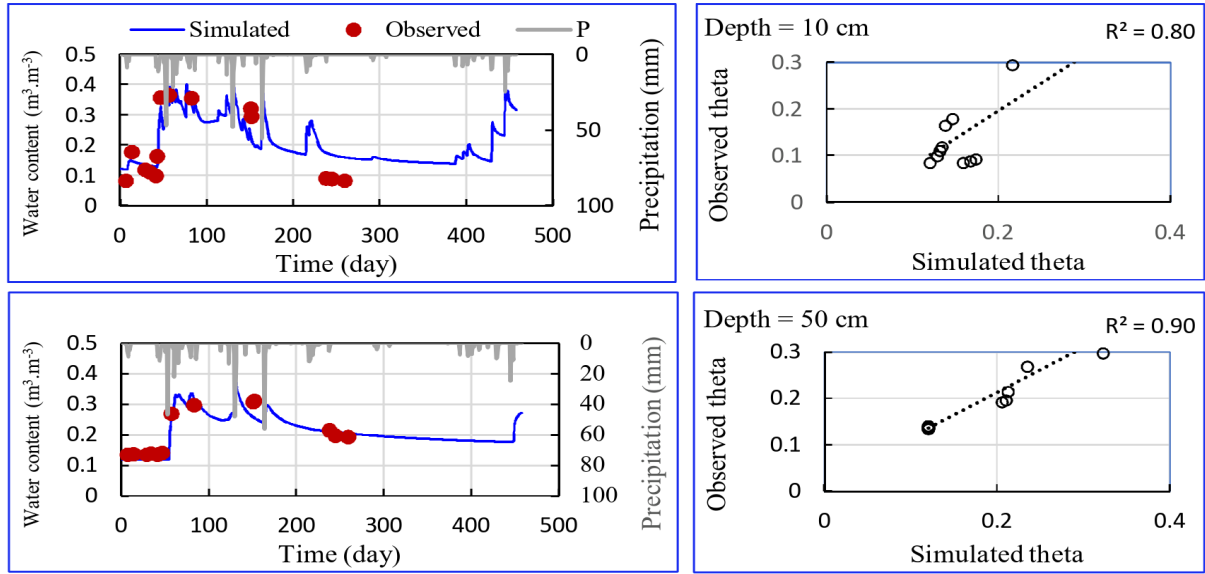


Figure 3) Soil water content variation, observed and simulated relation at the station 1

HYDRUS-1D model was selected to determine long-term water balance components in soil layers. The data collected from 7 stations calibrated the selected model based on two criteria: coefficient of determination and Root Mean Square Error (RMSE). The calibration results showed that the HYDRUS-1D can simulate SM dynamic. Therefore, the calibrated model was used to simulate the dynamic of SM with the data of boundary conditions for 15 years from the beginning of 2007 to the end of 2021. Table 6 shows the values of the parameters of the soil water retention curve along the soil profile at different stations based on the calibrated model. Table 6 shows that the saturated hydraulic conductivity of the soil varies

from 2 to 122 cm per day in the surface layer and from 6 to 18.5 cm per day in the lower layer of this area. In general, the hydraulic conductivity upstream is greater than that of the hydraulic conductivity downstream. The amount of drainage from the lower root zone was 10, 4, and 7.3 cm for rangeland, tree, and bare soils, respectively. The other results showed that infiltration was 42, 62, and 41 cm, and evapotranspiration was 317, 574, and 345 mm, respectively. This research showed that the highest amount of infiltration and SM storage occurred in tree land, the highest drainage from the root zone in the rangeland area, and the highest evaporation from the soil surface occurred in the bare soils.

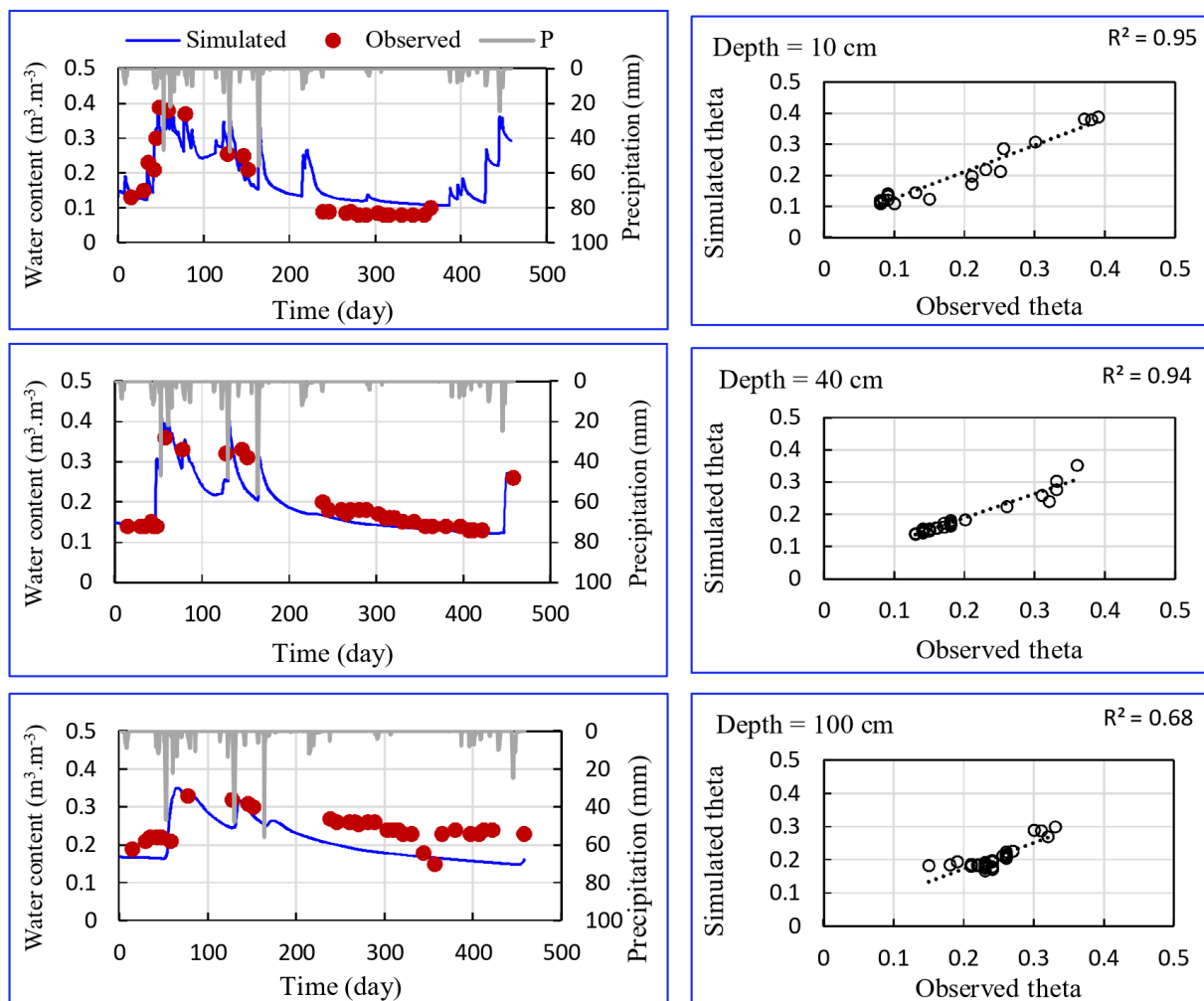


Figure 4) Soil water content variation, observed and simulated relation at the station 2.

Table 5) Correlation coefficient between simulated and observed SM at different sites.

Depth (m)	10	20	30	40	60	100
P1	0.80	--	--	--	0.90	--
P2	0.95	--	0.93	0.94	0.89	0.64
P3	0.59	0.57	0.84	0.94	0.81	0.61
P4	0.93	88	0.92	0.94	0.97	0.75
P6	0.97	0.91	0.87	0.94	--	0.8
P7	0.93	0.92	0.79	0.64	0.75	--

Table 6) The values of soil-water parameters of the model after the calibration stage.

Station	θ_r (cm ³ .cm ⁻³)	θ_s (cm ³ .cm ⁻³)	α (cm ⁻¹)	n (-)	Ks (cm.d ⁻¹)
P2-1	0.04	0.43	0.020	1.54	17.24
P2-2	0.04	0.52	0.017	2.45	2.82
P3-1	0.04	0.34	0.036	1.80	31.55
P3-2	0.04	0.52	0.024	2.24	3.5
P4-1	0.08	0.34	0.032	1.39	2.13
P4-2	0.091	0.44	0.010	1.19	0.87
P6-1	0.04	0.49	0.010	1.95	122.7
P6-2	0.04	0.52	0.023	1.56	18.50
P7-1	0.068	0.34	0.006	1.73	2.68
P7-2	0.04	0.52	0.005	2.48	0.59

Discussion

SM Content in the Soil Profile

Figure 7 shows the seasonal variation of SM storage during the simulation period at different stations over the watershed. The results of Figure 7 show that the P1 has a lesser soil moisture content than the other stations, which may be due to the lesser depth of the soil profile at this point (60 cm) relative to the other locations (100 cm). The amount of water storage and SM was generally similar at P2, P3, and P6, which have the same LC (rangeland). The mean of SM storage during the simulation period for the above sites was obtained as 19, 20, and 21 cm, respectively. The highest amount

of SM storage is due to P4 and P7, the area of the pine tree species and the bare soils, respectively. The mean of SM at P4 with tree LC was calculated as 30 cm, which is affected by an annual mean of four additional irrigations and rainwater catchments established around the trees. In general, the amount of SM in this station was higher than all other stations during the period of measurement and monitoring (Figures 3 to 6). Among the reasons for the higher moisture storage at this station, despite the more water use by tree species, is the effect of the rainwater catchment around the trees and SM capacity improved by tree roots. In the P7 Station, where the land-cover is bare soil, the mean SM store was 26 cm, which

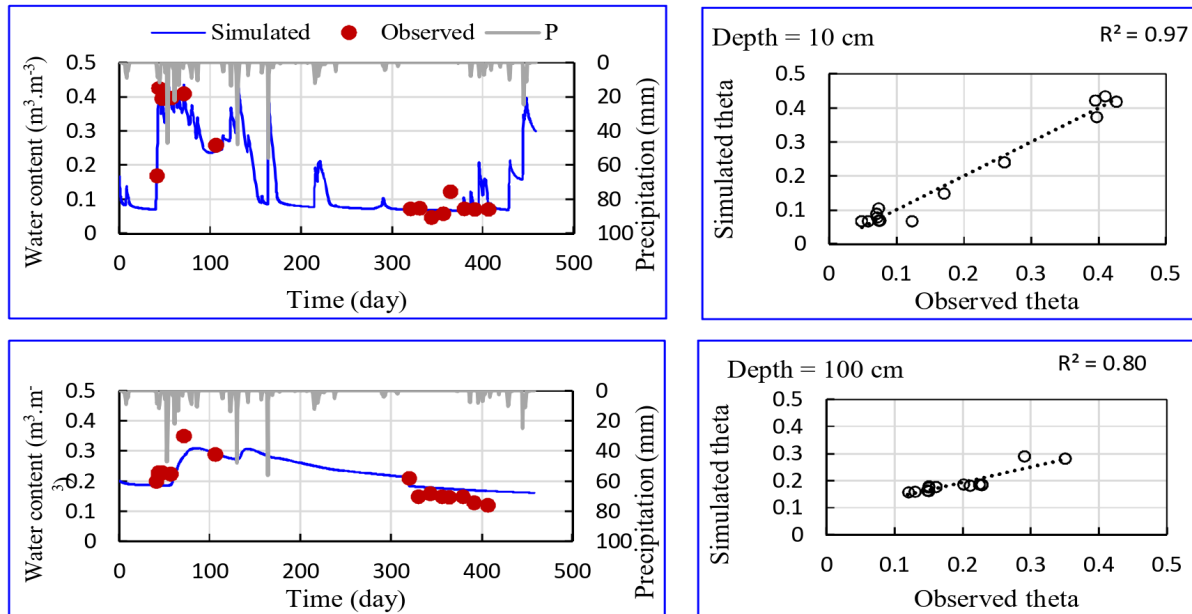


Figure 5) Soil water content variation, observed and simulated relation at the station 6

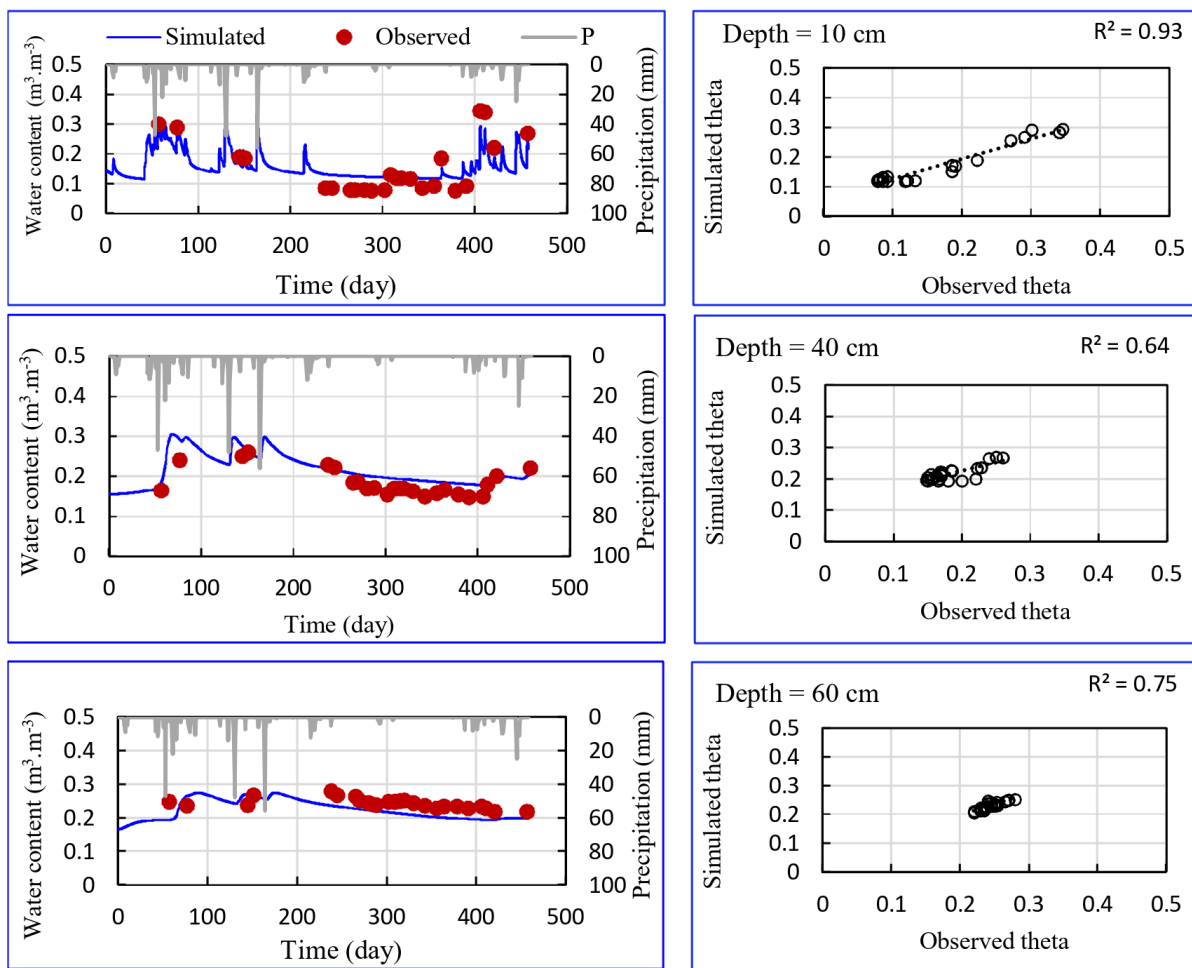


Figure 6) Soil water content variation, observed and simulated relation at the station 7

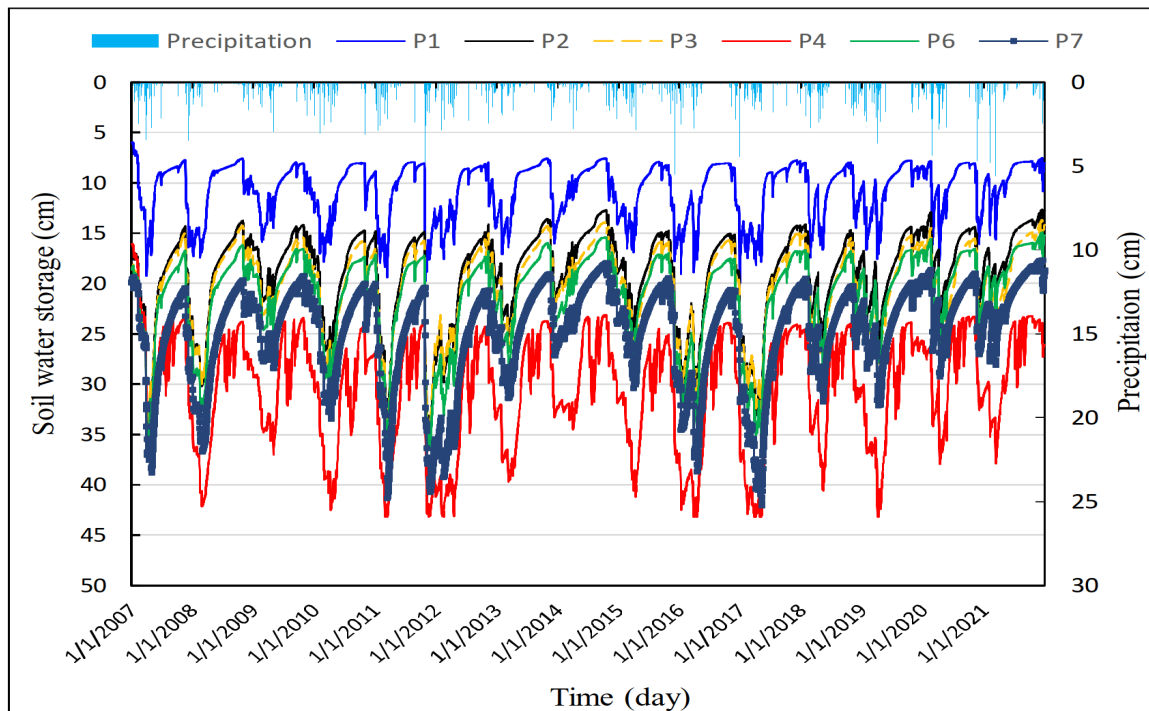


Figure 7) Variation of SM related to precipitation throughout the simulation period at various stations.

could relate to the absence of plants causing greater water retention.

Infiltration

The monthly infiltration from daily rainfall and supplementary irrigation was simulated for monitoring stations (Figure 8). The simulation results show that the amount of infiltration at stations P1, P2, P3, and P6, which had the same boundary conditions (rainfall, evaporation, and potential evapotranspiration), is almost equal. In addition, the cumulative infiltration is 625 cm, or the annual mean infiltration is 42 cm during this period. The cumulative infiltration amount in P7 with bare soil was estimated at 623 cm, slightly different from P1, P2, and P3. Conversely, the annual mean infiltration was estimated at 41.5 cm at this site. The cumulative infiltration in P4 is 935 cm, with an annual mean of 62 cm. P4 has the highest cumulative infiltration in this study area. The maximum annual infiltration occurred in 2011, and the minimum occurred in 2008. According to Figure 7, 2011 had

more rainfall than the other years, which is the reason for the increasing infiltration in this year.

The maximum infiltration occurred in November 2011, 16 cm at P4 and 14 cm at the other locations. The monthly infiltration at the station with the same LC and boundary conditions, including P1, P2, P3, and P6, are similar, and there are very few changes in station P7 with the same boundary conditions but different LCs (bare land). Figure 8 shows the monthly infiltration for P4 and P6 stations during the simulation period. Figure 7 shows cumulative infiltration values for points P1, P2, P3, P6, and P7, which are almost similar. According to the mentioned Figure, it is clear that the effect of supplementary irrigation in dry seasons increased the infiltration at the P4 station.

Runoff

The model estimates runoff based on the boundary conditions and soil moisture. If the rainfall rate is less than or equal to the infiltration capacity of the soil and the

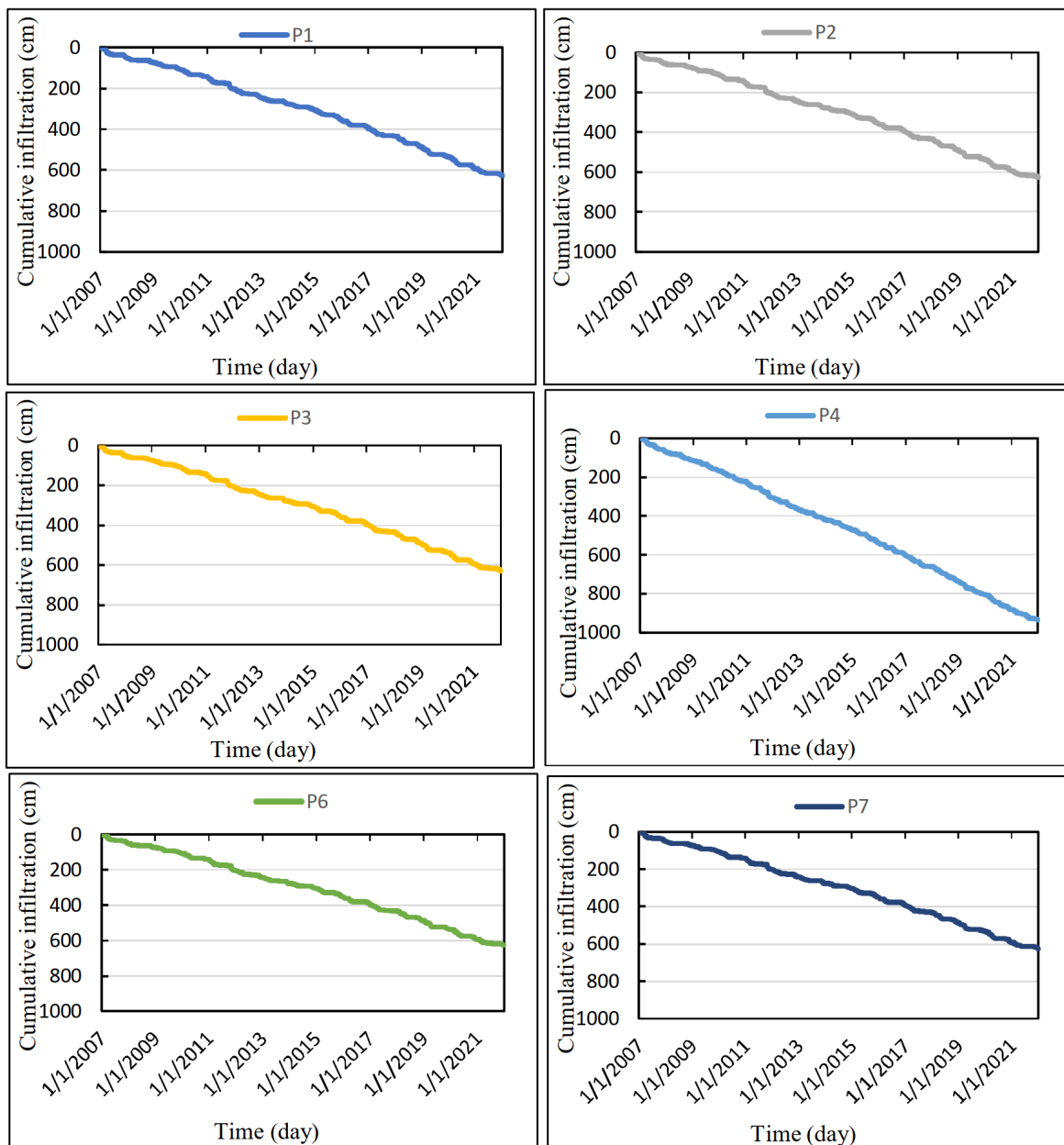


Figure 8) Cumulative infiltration during the simulation period at different stations.

evapotranspiration potential, runoff will not occur. Based on this, the estimated runoff by the model was zero in all places where the LC was rangeland or trees, but at P7 with bare soil, LC cumulative runoff was 13.2 cm from three events (Figure 9).

Evaporation and Transpiration

The model estimates actual evapotranspiration based on the potential evapotranspiration, rainfall (for all points), irrigation (only at point P4), and root water uptake. Table

7 shows cumulative and mean annual evapotranspiration for P1 to P6 and evaporation for P7 in the simulation period. The difference between actual evapotranspiration at any station with the same LC results from water uptake by the roots, which depends on the initial SM and soil water retention parameters. Therefore, in conditions with the same climate factors, the evapotranspiration process depends on the dynamic components of water in the soil. This result is compatible with Zhao

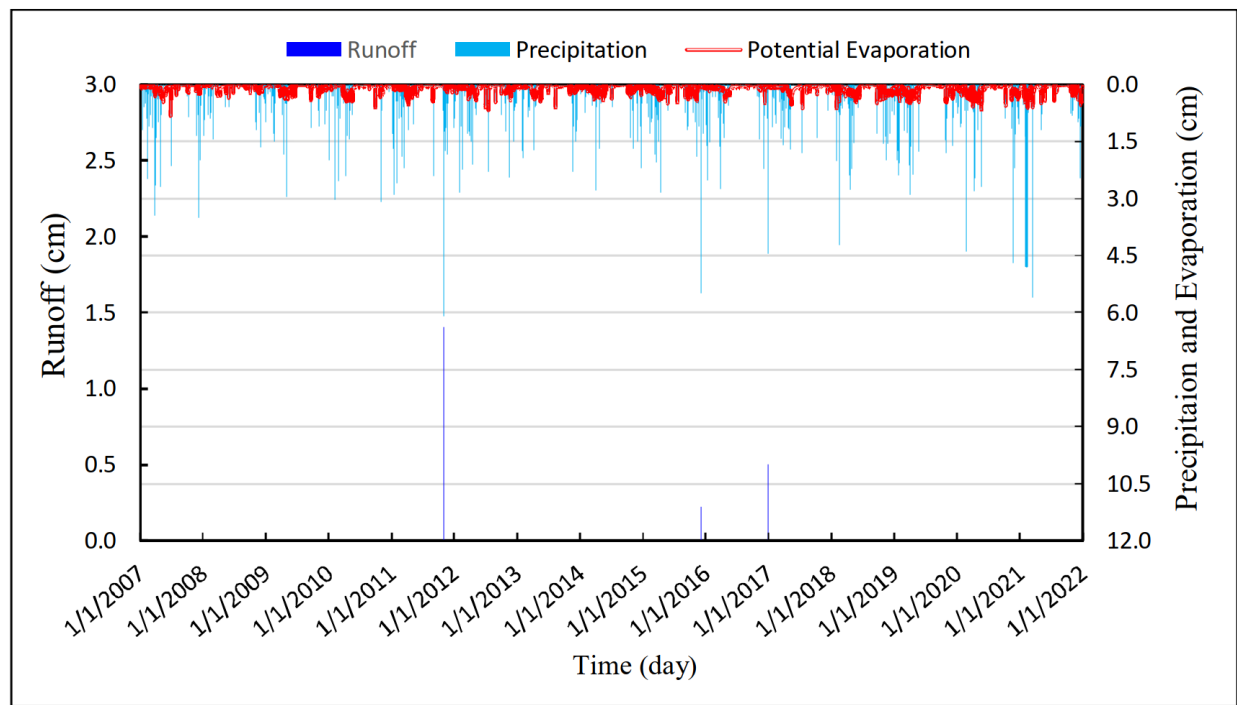


Figure 9) Simulated runoff compared to precipitation and potential evaporation at P7.

Table 7) Cumulative and mean annual evapotranspiration (mm) exhibits variation associated with different LCs.

Location	P1	P2	P3	P4	P6	P7
Cumulative Evapotranspiration	4760	4757	4352	8611	5208	5162
Mean annual evapotranspiration	317	317	290	574	347	345

et al. (2021) ^[74], whose research shows the double evapotranspiration in vegetated land related to the bare soils.

Drainage from Soil Bottom

Rainfall and irrigated water are the input for the model, and evaporation from the soil, transpiration by the plant, and SM storage changes are the outputs of the model. Therefore, if the remaining water is more than the field capacity of the soil, it gradually drains from the bottom of the soil profile. The model for different locations estimated the amount of drainage from the bottom of the soil column. The minimum soil drainage corresponds to P4, with LC as the tree species that could have more evapotranspiration. The highest amount of soil drainage corresponds to P3, with LC

as a rangeland. Also, the monthly variation of drainage for the monitoring stations is estimated by the model, presented in Table 8. The high amounts of soil drainage occurred in the wet months of the year. The fluctuation range of the drainage value at P1 is higher than that of the other stations, which may be due to the lesser depth of the soil profile, which will be more affected by atmospheric fluctuations. In general, in places where the land’s surface is covered by rangeland, the amount of drainage is higher than that of the other LC area, such as the tree LC (P4) or bare soil LC (P7). Therefore, land-cover, soil profile depth, and soil porosity control drainage from the lower part of the soil depth and the state of the subsurface flow in such areas.

Table 8) Drainage from soil bottom at different stations (cm) for different LCs.

Station	Cumulative Drainage Value	Mean Annual	Range of Drainage Change	Monthly Mean
P1	151	10	0 - 10.5	0.85
P2	155	10.3	0.12 - 6.1	0.86
P3	193	13	0.18 - 6.4	1
P4	61	4	0 - 8	0.34
P6	107	7	0.06 - 5.2	0.6
P7	109	7.3	0.12 - 3	0.6

Conclusion

This research aimed to investigate the SM dynamic on the watershed scale. For this purpose, six soil moisture monitoring stations were established in the Telo Watershed, located east of Tehran City, based on the different LCs, including natural rangeland, tree species, and areas without vegetation or bare soils. Then, soil moisture monitoring tools and equipment are installed in these stations at depths of 10, 20, 30, 40, 60, and 100 cm from the ground surface. These monitoring stations collected data for 18 months, from October 2018 to April 2022. One monitoring station (P4) was considered in the tree LC, four stations (P1, P2, P3, and P6) for natural rangelands in different elevations and valleys, and one station (P7) in the bare soil area. The observed data were used to calibrate the HYDRUS-1D, and the coefficient of determination (R^2) and the Root Mean Square Error (RMSE) were selected as criteria for assessing correlation relationships. SM dynamic was simulated by the calibrated model over a long-term period from early 2007 to late 2021 to estimate the soil water balance components at different LU areas. Then, water retention curve parameters were optimized using the calibrated model. As a key parameter of the soil water retention curve, the saturated hydraulic conductivity values range from 2

to 122 cm per day in the surface layer and from about 0.6 to 18.5 cm per day in the lower layer over the watershed.

The first result shows that the mean soil moisture storage is 30, 20, and 26 cm for different LCs, including trees, rangeland, and bare soil. The annual mean drainage values from the bottom of the soil column for tree (P4), rangeland (P1, P2, P3, and P6), and bare soil (P7) LC obtained as 4, 10, and 7.3 cm per year, respectively. Also, the annual mean of actual evapotranspiration for these three types of LC is 574, 317, and 345 mm, respectively. In addition, surface runoff is low and insignificant for tree and rangeland areas. The annual mean infiltration from rainfall is 62, 42, and 41.5 cm per year, respectively. Therefore, the type of LC is the main factor in controlling the distribution of the water balance components and the SM storage at the boundary conditions of the surface and subsurface flow dynamic. The trees and the rangeland-type LC in this boundary layer have increased soil permeability and moisture storage capacity. Also, the maximum evaporation from the soil surface is in the bare soil, but evapotranspiration is in the tree LC. Our results align with those of Zhao et al. (2021) ^[74], which indicate that double evapotranspiration occurs in vegetated land compared to bare soils. Furthermore, our findings are consistent

with ^[49], which shows that in tree cover, evapotranspiration increases while deep percolation decreases about shrub cover. The behavior of different LCs on the amount of drain water from the base of the soil column, which supplies deep percolation and subsurface flows, is ambiguous as the orders are rangeland lands, bare soils, and tree LC, respectively, which may be due to the water absorption by tree roots and increasing evapotranspiration in the area with tree LC relative to the other LC. This means that the tree's root system improved soil infiltration and storage capacity, but it did not mean that deep percolation increased from soil covered by trees. In general, the results of this research show that the type of LC and LU had a crucial role in controlling the water balance components and SM dynamic. Therefore, the knowledge of the type of LC and LU is necessary for managing water resources and uses, as well as LU change programs. Finally, the influence of LU and LC must be considered regarding water balance components, particularly the spatial and temporal distribution of soil moisture dynamic, in managing and utilizing water resources. This research concentrated exclusively on the effects of three LU/LC types on soil moisture dynamic. Consequently, it is advised that future studies also examine the impacts of additional LU/LC types and enhance the density of monitoring stations.

Acknowledgment

The authors wish to thank all who assisted in conducting this work. The authors acknowledge with grateful appreciation the kind assistance and financial support provided by the Soil Conservation and Watershed Management Research Institute (SCWMRI) and Pardis Company of Iran. The Meteorological Organization of IR Iran is thanked for providing long-term precipitation, evaporation, and temperature data.

Funding: Soil Conservation and Watershed Management Research Institute (SCWMRI) and Pardis Company of Iran supported this work.

Conflicts of Interests: The authors have no relevant financial or non-financial interests to disclose.

Authors Contributions: **J Porhemmat:** Conceptualization, Methodology, Software, Formal analysis, Data curation, Writing, and original draft preparation, Visualization, Investigation, Validation, Writing-Reviewing and Editing the final draft; **SM Tajbakhsh:** Validation, Writing-Reviewing and Editing the final draft, and original draft preparation, Data curation; **M Altafi Dadgar:** Software, Formal analysis, Data curation, Data collection; **AA Kolahchi:** Reviewing and Editing the final draft, Data curation, Investigation, Data collection **Ethical permissions:** No ethical approval was required for this study.

References

1. Hu W., Shao M.A., Hou M.T., She D.L., Si B.C. Mean soil water content estimation using measurements from time stable locations of adjacent or distant areas. *J. Hydrol.* 2013; 497 (1):234-243.
2. Vereecken H., Huisman J.A., Pachepsky Y., Montzka C., van der Kruk J., Bogen H., Weihermüller L., Herbst M., Martinez G., Vanderborght J. On the spatio-temporal dynamics of soil moisture at the field scale. *J. Hydrol.* 2014; 516(4): 76-96.
3. Rasheed M.W., Tang J., Sarwar A., Shah S., Saddique N., Khan M.U., Imran Khan M., Nawaz S., Shamshiri R.R., Aziz M., Sultan M. Soil moisture measuring techniques and factors affecting the moisture dynamics: A comprehensive review. *Sustainability.* 2022; 14(18): 11538.
4. Ye N., Walker J.P., Gao Y., Pop Stefaniya I., Hills J. Comparison between thermal-optical and L-band passive microwave soil moisture remote sensing at farm scales: Towards UAV-based near-surface soil moisture mapping. *IEEE J. Sel. Top. Appl. Earth Obs. Remote Sens.* 2024; 17(1): 633-642.
5. Zhang M., Zhang D., Jin Y., Wan X., Ge Y. Evolution of soil moisture mapping from statistical models to integrated mechanistic and geoscience-aware approaches. *Inf.Geogr.* 2025; 1(1): 100005.

6. Widyastuti M.T., Padarian J., Minasny B., Webb M., Taufik M., Kidd D. Mapping near-real-time soil moisture dynamics over Tasmania with transfer learning. *Soil*. 2025; 11(1): 287–307.
7. Bakhshian S., Zarepakzad N., Nevermann H., Hohenegger C., Or D., Shokri N. Field-scale soil moisture dynamics predicted by deep learning. *Adv. Water Resour.* 2025; 201: 104976.
8. Ursulino B.S., Montenegro S.M.G.L., Coutinho A.P., Coelho V.H.R., Araújo D.C.D.S., Gusmão A.C.V., Neto S.M.D.S., Lassabatere L., Angulo-Jaramillo R. Modelling soil water dynamics from soil hydraulic parameters estimated by an alternative method in a tropical experimental basin. *Water*. 2019; 11(1): 1007
9. Duarte E., Hernandez A. A review on soil moisture dynamics monitoring in semi-arid ecosystems: methods, techniques, and tools applied at different scales. *Appl. Sci.* 2024; 14(17): 7677.
10. Vereecken H., Huisman J.A., Hendricks Franssen H.J., Brüggemann N., Bogaen H.R., Kollet S., Javaux M., van der Kruk J., Vanderborght J. Soil hydrology: Recent methodological advances, challenges, and perspectives. *Water Resour. Res.* 2015; 51(4): 2616-2633.
11. Bai X., Jia X., Jia Y., Shao M., Hu W. Modeling long-term soil water dynamics in response to land-use change in a semi-arid area. *J. Hydrol.* 2020; 585: 124824.
12. Cantón Y., Solé-Benet A., Domingo F. Temporal and spatial patterns of soil moisture in semi-arid badlands of SE Spain. *J. Hydrol.* 2004; 285(1–4): 199-214.
13. Jafarian Jeloudar Z., Shabanzadeh S., Kavian A., Shokri M. Spatial variability of soil features affected by land use type using geostatistics. *ECOPERSIA* 2014; 2(3): 667-679.
14. Shen M., Zhang J., Zhang S., Zhang H., Sun R., Zhang Y. Seasonal variations in the influence of vegetation cover on soil water on the loess hillslope. *J. Mt. Sci.* 2020; 17(9): 2148–2160.
15. Jia X., Wang Y., Shao M., Luo Y., Zhang C. Estimating regional losses of soil water due to the conversion of agricultural land to forest in China's Loess Plateau. *Ecohydrology*. 2017b; 10(6): e1851.
16. Afshari M., Hashemi S.S., Attaeian B. Land use change effect on physical, chemical, and mineralogical properties of calcareous soils in western Iran. *ECOPERSIA* 2019; 7(1):47-57.
17. Jia X., Zhao C., Wang Y., Zhu Y., Wei X., Shao M. Traditional dry soil layer index method overestimates soil desiccation severity following conversion of cropland into forest and grassland on China's Loess Plateau. 2020; 291: 106794.
18. Porhemmat J., Nakhaei M., Altafi Dadgar M., Biswas A. Investigating the effects of irrigation methods on potential groundwater recharge: A case study of semi-arid regions in Iran. *J. Hydrol.* 2018; 565(1): 455-466.
19. Altafi Dadgar M., Nakhaei M., Porhemmat J., Eliasi B., Biswas A. Potential groundwater recharge from deep drainage of irrigation water. *Sci. Total Environ.* 2020; 716: 137105.
20. Garcia-Prats A., del Campo A.D., Pulido-Velazquez M. A hydroeconomic modeling framework for optimal integrated management of forest and water. *Water Resour. Res.* 2016; 52(10): 8277-8294.
21. Jarvis N. J. Simulation of soil water dynamics and herbicide persistence in a silt loam soil using the MACRO model. *Ecol. Modell.* 1995; 81(1-3): 97-109.
22. Jarvis N.J., Messing I. Near-saturated hydraulic conductivity in soils of contrasting texture as measured by tension infiltrometers. *Soil Sci. Soc. Am. J.* 1995; 59(1): 27-34.
23. Jarvis N.J., Hollis J.M., Nicholls P.H., Mayr T., Evans S.P. MACRO—DB: a decision-support tool for assessing pesticide fate and mobility in soils. *Environ. Model. Softw.* 1997; 12(2-3): 251-265.
24. Fechter J., Allison B.E., Sivakumar M.V.K., Van Der Ploeg R.R., Bley J. An evaluation of the SWATRER and CERES-Millet models for southwest Niger. *IAHS Publ.* 1991; 199(1): 505-513.
25. J.G., Feddes R.A., Kabat P., van Walsum P.E.V., Groenendijk P., van Diepen C.A. Theory of SWAP version 2.0; simulation of water flow, solute transport and plant growth in the soil-water-atmosphere-plant environment. Report 71, Department Water Resources, Wageningen Agricultural University. 1997; 71: 167pp.
26. Van Dam J.C. Field scale water flow and solute transport: SWAP model concepts, parameter estimation, and case studies. Ph.D. diss., Wageningen Univ., the Netherlands. 2000: 167pp.
27. Hutson J.L., Wagenet R.J. LEACHM: Leaching, estimation and chemistry model: A process-based model of water and solute movement, transformations, plant uptake and chemical reactions in the unsaturated zone, Version 2, Department of Agronomy, Cornell University, Ithaca, N.Y. 1989: 148 pp.
28. Hutson J. L., Wagenet R.J. Simulating nitrogen dynamics in soils using a deterministic model.

- Soil Use Manage. 1991; 7(1): 74–78.
29. Hutson J.L. Leaching Estimation and Chemistry Model: A Process-Based Model of Water and Solute Movement, Transformations, Plant Uptake, and Chemical Reactions in the Unsaturated Zone. Version 4, Department of Crop and Soil Sciences, Research Series No. R03–1, Cornell University, Ithaca, NY, USA 2003.
 30. Asada K., Eguchi S., Urakawa R., Itahashi S., Matsumaru T., Nagasawa T., Aoki K., Nakamura K., Katou H. Modifying the LEACHM model for process-based prediction of nitrate leaching from cropped Andosols. *Plant Soil*. 2013; 373(1): 609–625.
 31. Šimůnek J., Šejna M., van Genuchten M.Th. The HYDRUS-2D software package for simulating the two-dimensional movement of water, heat, and multiple solutes in variably-saturated media. U.S. Salinity Laboratory. Agricultural Research Service, Riverside, California. 1999:240p.
 32. Šimůnek J., van Genuchten M.Th., Šejna M. The HYDRUS-1D Software package for simulating the one-dimensional movement of water, heat, and multiple solutes in variably-saturated media, Version 3.0. Department of Environmental Sciences, University of California Riverside, Riverside, California. 2005:240p.
 33. Šimůnek J., Šejna M., van Genuchten M.Th. The HYDRUS software package for simulating two- and three-dimensional movement of water, heat, and multiple solutes in variably-saturated media. User Manual, Version 1.0, PC Progress, Prague, Czech Republic. 2006 :241p.
 34. Šimůnek J., Šejna M., Saito H., Sakai M., van Genuchten M.Th. The HYDRUS-1D software package for simulating the one-dimensional movement of water, heat, and multiple solutes in variably-saturated media, Version 4.08. Department of Environmental Sciences University of California Riverside, Riverside, California. 2009 :240p.
 35. Šimůnek J., Van Genuchten M.Th., Šejna M. HYDRUS: Model use, calibration, and validation. *Trans. ASABE*. 2012; 55(4): 1261-1274.
 36. Šimůnek J., Šejna M., Saito H., Sakai M., van Genuchten M.Th. The HYDRUS-1D Software Package for Simulating the One-Dimensional Movement of Water, Heat, and Multiple Solutes in Variably-Saturated Media. Version 4.17, Department of Environmental Sciences, University of California, California, USA. 2013: p308.
 37. Šimůnek J., van Genuchten M.Th., Šejna M. Recent developments and applications of the HYDRUS-1D computer software packages. *Vadose Zone J*. 2016; 15(7): 1-25.
 38. Radcliffe D.E., Šimůnek J. *Soil Physics with HYDRUS: Modeling and Applications*. 1st Edition, CRC Press. 2018: 388 pp.
 39. Richards Lisa A. Capillary conduction of liquids through porous mediums, *J. Appl. Phys.* 1931; 1 (1): 318-333.
 40. Abbasi F., Adamsen F.J., Hunsaker D.J., Feyen J., Shouse P., van Genuchten M.Th. Effects of flow depth on water flow and solute transport in furrow irrigation: Field data analysis. *J. Irrig. Drain. Eng.* 2003; 129(4): 237-254
 41. Wang F.X., Kang Y., Liu S.P. Effects of drip irrigation frequency on soil wetting pattern and potato growth in North China Plain. *Agric. Water Manag.* 2006; 79(3): 248-264.
 42. Skaggs T. H., Trout T. J., Šimůnek J., Shouse P. J. Comparison of HYDRUS-2D simulations of drip irrigation with experimental observations. *J. Irrig. Drain. Eng.* 2004; 130(4): 304-310.
 43. Wöhling T. Seasonal Furrow Irrigation Modelling with HYDRUS2: In *Proceedings of Workshop on HYDRUS Applications*. October 19, 2005, Department of Earth Sciences Utrecht University, The Netherlands: 74-77.
 44. Siyal A.A., Skaggs T.H. Measured and simulated soil wetting patterns under porous clay pipe subsurface irrigation. *Agric. Water Manag.* 2009; 96(6): 893-904.
 45. Patel N., Rajput T.B.S. Dynamics and modeling of soil water under subsurface drip irrigated onion. *Agric. Water Manag.* 2008; 95(12): 1335-1349.
 46. Cheng X., Huang M., Si B.C., Yu M., Shao M. The differences of water balance components of *Caragana korshinskii* grown in homogeneous and layered soils in the desert-Loess Plateau transition zone. *J. Arid Environ.* 2013; 98(1): 10-19.
 47. Essig E.T., Corradini C., Morbidelli R., Govindaraju R.S. Infiltration and deep flow over sloping surfaces: Comparison of numerical and experimental results. *J. Hydrol.* 2009; 374(1-2): 30-42.
 48. Guan H., Šimůnek J., Newman B.D., Wilson J.L. Modelling investigation of water partitioning at a semi-arid ponderosa pine hillslope. *Hydrol. Process.* 2010; 24(9): 1095-1105.
 49. Wang H., Tetzlaff D., Soulsby C. Modelling the effects of land-cover and climate change on soil water partitioning in a boreal headwater

- catchment. *J. Hydrol.* 2018; 558(1): 520–531.
50. Besharat S., Nazemi A.H., Sadraddini A.A. Shahmorad S. Applications of HYDRUS and the proposed SWMRUM software in simulating water flow with root water uptake through soils. *Water Soil Sci.* 2011; 21(4): 121-137.
 51. Altafi Dadgar M., Nakhaei M., Porhemmat J., Biswas A., Rostami M. Transient potential groundwater recharge under surface irrigation in semi-arid environment: An experimental and numerical study. *Hydrol. Process.* 2018; 32(25): 3771-3783.
 52. Noorabadi S., Sadraddini S.A.A., Nazemi A.H., Delirhasannia R. Application of the SIRMOD and HYDRUS-3D Models to Completely Simulate the Furrow Irrigation Process. *Iranian J. Irrig. Drain.* 2014; 8(3): 443-452.
 53. Xiaoxu J., Shao M., Zhu Y., Luo Y. Soil moisture decline due to afforestation across the Loess Plateau, China. *J. Hydrol.* 2017; 546: 113-122.
 54. Elnesr M.N., Alazba A.A. Computational evaluations of HYDRUS simulations of drip irrigation in 2D and 3D domains (i-Surface drippers). *Comput. Electron. Agr.* 2019; 162(1): 189-205.
 55. Forkutsa I., Kaas R.S. Shirokova Y.I., Lamers J.P.A., Kienzler K., Tischbein B., Martius C., Vlek P.L.G. Modeling irrigated cotton with shallow groundwater in the Aral Sea Basin of Uzbekistan: I. water dynamics. *Irrig. Sci.* 2009; 27(1): 331-346. DOI:
 56. Šimůnek J., van Genuchten M.Th., Sejna M. Development and applications of the HYDRUS and STANMOD software packages and related codes. *Vadose Zone Journal* 2008; 7(2): 587-600.
 57. Xie T., Liu X., Sun T. The effects of groundwater table and flood irrigation strategies on soil water and salt dynamics and reed water use in the Yellow River Delta, China. *Ecol. Model.* 2011; 222(2): 241-252.
 58. Djabelkhir K., Lauvernet C., Kraft P., Carlier N. Development of a dual permeability model within a hydrological catchment modeling framework: 1D application. *Sci. Total Environ.* 2017; 575(1): 1429-1437.
 59. Hu W., Wang Y.Q., Li H.J., Huang M.B., Hou M.T., Li Z., She D.L., Si B.C. Dominant role of climate in determining spatio-temporal distribution of potential groundwater recharge at a regional scale. *J. Hydrol.* 2019; 578: 124042.
 60. Guo Y., Fang G., Xu Y P., Tian X., Xie J. Identifying how future climate and LU/cover changes impact streamflow in Xinjiang Basin, East China. *Sci. Total Environ.* 2020; 710: 136275.
 61. Zhang C., Wang Y., Jia X., Shao M., An Z. Variations in capacity and storage of plant-available water in deep profiles along a revegetation and precipitation gradient. *J. Hydrol.* 2020; 581: 124401.
 62. Porhemmat J., Altafi-Dadgar M., Abdolnabi Abdeh-Kolahchi A. Modeling long-term soil water dynamics in response to land use changes: Pilot study of Telo region. *SCWMRI*, 2023; 64810: 73 pp.
 63. Grossman R.B., Reinsch T.G. Bulk density, and linear extensibility: Core Method. In: Dane, J.H. and Topp, G.C. (Eds.), *Methods of Soil Analysis, Part 4, SSSA Book Series*. American Society of Agronomy, Madison. 2002; WI: 201–228.
 64. Dane J.H., Hopmans J.W. Pressure plate extractor. In: Dane, J., Topp, C (Ed.), *Methods of Soil Analysis, Part 4, SSSA Book Series*. American Society of Agronomy, Madison. 2002; WI: 688–690.
 65. Gee G.W., Or D. Particle size analysis. In: Dane, J.H. and Topp, G.C., (Eds.), *Methods of Soil Analysis, Part 4, Physical Methods, Soils Science Society of America, Book Series No. 5*, Madison. 2002: 255-293.
 66. Feddes R.A., Kowalik P.J., Zaradny H. *Simulation of Field Water Use and Crop Yield*. John Wiley & Sons. 1978: 189pp.
 67. Van Genuchten M.Th. A closed-form equation for predicting the hydraulic conductivity of unsaturated soils. *Soil Sci. Soc. Am. J.* 1980; 44(5): 892-898.
 68. Mualem Y. A new model for predicting the hydraulic conductivity of unsaturated porous media. *Water Resour. Res.* 1976; 12(3): 513-522.
 69. Turkeltaub T., Kurtzman D., Bel G., Dahan O. Examination of groundwater recharge with a calibrated/validated flow model of the deep vadose zone. *J. Hydrol.* 2015; 522(1): 618-627.
 70. Kashyap P.S., Panda R.K. Evaluation of evapotranspiration estimation methods and development of crop-coefficients for potato crop in a sub-humid region. *Agric. Water Manag.* 2001; 50(1): 9-25.
 71. Allen R.G., Pereira L.S., Raes D., Smith, M. *Crop evapotranspiration - guidelines for computing crop water requirements*. FAO Irrigation and Drainage Paper. 56, FAO, 1998, ISBN 92-5-104219-5.
 72. Jiménez-Martínez J., Skaggs T.H., van Genuchten M.Th., Candela L. A root zone modelling approach

- to estimating groundwater recharge from irrigated areas. *J. Hydrol.* 2009; 367(1): 138-149.
73. Schaap M.G., Leij F.J., van Genuchten M.Th. Rosetta: A computer program for estimating soil hydraulic parameters with hierarchical pedotransfer functions. *J. Hydrol.* 2001; 251(3-4): 163-176.
74. Zhao M., Wang W., Ma Z., Wang Q., Wang Z., Chen L., Fu B. Soil water dynamics based on a contrastive experiment between vegetated and non-vegetated sites in a semi-arid region in Northwest China. *J. Hydrol.*, 2021; 603A: 126880.